Antiferromagnetic order in the honeycomb Kondo lattice $CePt_6Al_3$ induced by Pd substitution

R. Oishi,[1] K. Umeo,[2] Y. Shimura,[1] T. Onimaru,[1] A. M. Strydom,[3] and T. Takabatake[1,*]

[1]*Department of Quantum Matter, Graduate School of Advanced Science and Engineering, Hiroshima University, Higashi-Hiroshima 739-8530, Japan*

[2]*Department of Low Temperature Experiment, Integrated Experimental Support/Research Division, Natural Science Center for Basic Research and Development (N-BARD), Hiroshima University, Higashi-Hiroshima 739-8526, Japan*

[3]*Highly Correlated Matter Research Group, Physics Department, University of Johannesburg, Auckland Park 2006, South Africa*

(Received 26 June 2021; revised 23 August 2021; accepted 25 August 2021; published 7 September 2021)

The cerium-based compound $CePt_6Al_3$, in which Ce atoms form a honeycomb lattice hosting magnetic frustration, has a heavy-fermion ground state. We have observed development of magnetic order in partially Pd-substituted $Ce(Pt_{1-x}Pd_x)_6Al_3$ series up to $x = 0.3$ by the measurements of magnetic susceptibility, electrical resistivity ρ, and specific heat C. In the whole range of x, the unit cell volume remains unchanged within 0.2%, and the effective magnetic moment stays at 2.4 μ_B/Ce. For $x = 0.05$, both C/T and $\rho(T)$ jump on cooling at $T_m = 1.8$ K. With increasing x to 0.2, T_m increases to 3.8 K, where C/T shows a pronounced λ-type anomaly. Application of magnetic fields suppresses T_m, which is indicative of an antiferromagnetic (AFM) ordered state. Thus, a long-range AFM order is induced by the substitution of isovalent Pd for Pt in $CePt_6Al_3$ without carrier doping and chemical pressure. We attribute the emergence of AFM order in $Ce(Pt_{1-x}Pd_x)_6Al_3$ to the randomness in the spin-orbit interaction in the Pt-Pd sublattice, which weakens both the coherent Kondo effect and magnetic frustration in the honeycomb Kondo lattice.

DOI: 10.1103/PhysRevB.104.104411

I. INTRODUCTION

Magnetic frustration in insulators with honeycomb lattices as well as triangular and kagome lattices has long been investigated because they are thought as possible candidates for quantum spin liquids [1,2]. Recently, this research field has been activated by the advent of the Kitaev model which postulates bond-directional anisotropic exchange interactions between nearest-neighbor (NN) spins on a honeycomb lattice [3,4]. However, geometrical frustration in metallic lattices is less obvious because magnetic interactions are long ranged, as exemplified by the Ruderman-Kittel-Kasuya-Yosida (RKKY) interaction in rare-earth-based intermetallic compounds [5]. The lack of local inversion symmetry at the rare-earth site in the honeycomb lattice leads to an odd-parity crystal electric field (CEF) which mixes the $4f$ and $5d$ orbitals of the rare-earth ion. The local parity mixing together with the antisymmetric spin-orbit coupling is prone to induce a complex magnetic order such as a coplanar vortex-lattice-type magnetic order [6,7]. In Ce- and Yb-based intermetallic compounds, moreover, the RKKY interaction competes with the Kondo interaction by which spin polarization of conduction electrons screens the $4f$ magnetic moment [8]. Theoretically, the interplay between geometrical frustration, RKKY interaction, and Kondo effect gives rise to various states including a spin-density-wave (SDW) state, a local moment antiferromagnetic (AFM) ordered state, an AFM state coexisting with fractionalized excitations, and a partial Kondo screened state with site-dependent moment size [9–12]. Such a situation is expected to be realized in a Ce- or Yb-honeycomb compound where a doublet ground state under CEF can be described as an effective $\frac{1}{2}$ spin.

To investigate the interplay in the honeycomb Kondo lattice, the recently reported Ce-based compound $CePt_6Al_3$ is an ideal candidate which crystallizes in the $NdPt_6Al_3$-type trigonal structure with a centrosymmetric space group $R\bar{3}c$ [13]. In the layered structure shown in Fig. 1(a), a triangle of Pt_3 centers a Ce hexagon. A flat Ce_2Pt_3 layer and a Pt_9Al_6 block, which is omitted in Fig. 1(a), are alternatively sixfold stacked along the c axis in the unit cell having a large ratio $c/a = 5.2$. The NN and next-NN (NNN) Ce-Ce distances in the honeycomb plane are $d_1 = 4.36$ Å and $d_2 = 7.55$ Å, respectively, the latter of which is longer than the interplane Ce-Ce distance of $d_3 = 6.58$ Å. However, the number of Ce atoms at the distance of d_3 is only one, much smaller than eight for that at the distance of d_2. Therefore, the interlayer magnetic interaction should be much weaker than the intralayer interaction.

The physical properties of $CePt_6Al_3$ have been studied on single-crystalline samples by the measurements of magnetic susceptibility χ, electrical resistivity ρ, and specific heat C [14]. Rather weak anisotropy in $\chi(T)$ and $\rho(T)$ was observed despite the layered crystal structure. The trivalent state of the Ce ion was indicated by the effective magnetic moment $\mu_{\rm eff}$ of 2.41 μ_B/Ce for both directions of magnetic field $B//c$ and $B\perp c$. The analysis of the magnetic entropy revealed a doublet CEF ground state which is separated by ∼100 K from a quasidegenerated quartet excited state. On cooling, C/T passes through a broad maximum of 0.5 J/K^{2}mol at 0.55 K while $\rho(T)$ decreases as T^2 down to 0.05 K without

*takaba@hiroshima-u.ac.jp

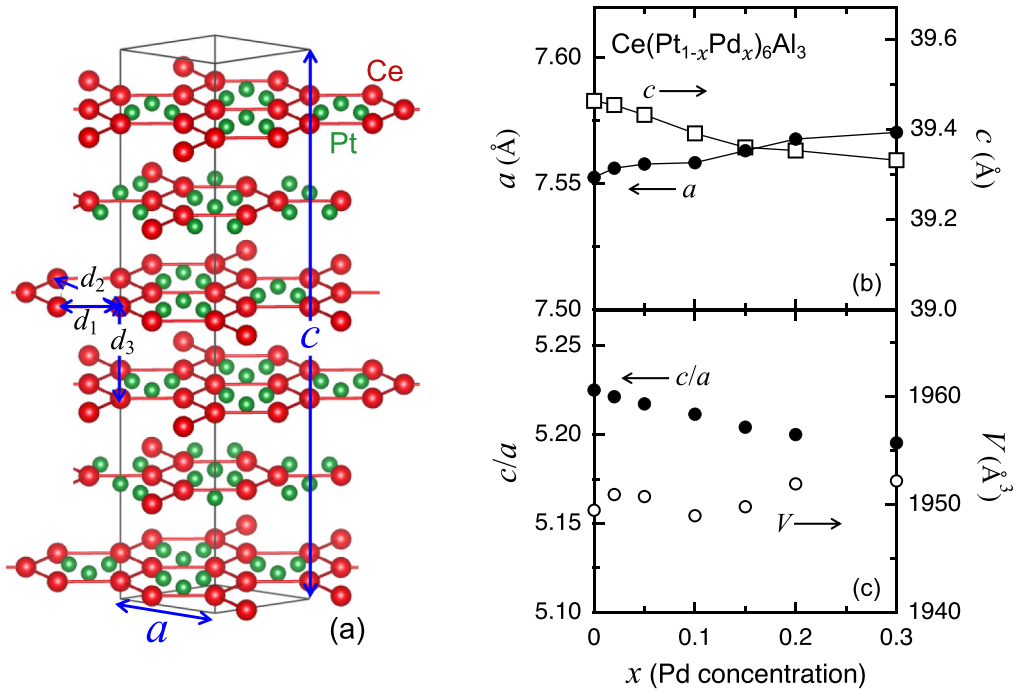

FIG. 1. (a) Layers of Ce (red) honeycombs with Pt (green) triangles on the center which are stacked along the c axis in $CePt_6Al_3$ of the trigonal $NdPt_6Al_3$-type structure [13]. Pt_9Al_6 blocks between the Ce_2Pt_3 layers are omitted for clarity. Intralayer Ce-Ce distances are denoted as d_1 and d_2 and the interlayer distance as d_3 (see text). (b) Trigonal lattice parameters a and c and (c) the ratio c/a and the unit cell volume V for $Ce(Pt_{1-x}Pd_x)_6Al_3$ as a function of the Pd concentration x.

showing any anomaly. These physical properties classified $CePt_6Al_3$ as a nonmagnetic heavy-fermion system, while the role of frustration in the formation of the heavy-fermion state remains obscure [14].

In this paper, we intend to reveal the role of frustration by studying the physical properties of $Ce(Pt_{1-x}Pd_x)_6Al_3$, where the isovalent Pd atom is partially substituted for the Pt atom. Because the metallic radius of Pd (1.37 Å) is close to that of Pt (1.39 Å) [15], a chemical pressure effect on the Ce $4f$ state would be weak. On the other hand, the atomic mass of Pd is $\sim \frac{1}{2}$ of that of Pt. This difference in the atomic mass would strongly reduce the spin-orbit interaction of the d band derived from Pt $5d$ and Pd $4d$ states, as pointed out for $Ce_3Bi_4(Pt_{1-x}Pd_x)_3$ [16]. The randomness in the spin-orbit interaction in $Ce(Pt_{1-x}Pd_x)_6Al_3$ may modify not only the onsite Kondo interaction between the $4f$ state and d states but also the periodically oscillating RKKY interaction mediated by the d band.

II. EXPERIMENTS

Polycrystalline samples with initial compositions of $Ce(Pt_{1-x}Pd_x)_6Al_3$ ($X = 0$, 0.02, 0.05, 0.10, 0.15, 0.2, 0.3, and 0.4) were prepared by arc-melting appropriate amounts of constituent elements Ce (99.9%), Pt (99.95%), Pd (99.99%), and Al (99.999%) under a purified argon atmosphere. To improve the homogeneity, the ingots were turned over and melted several times. The samples were subsequently annealed for 10 d in evacuated quartz ampoules at temperatures between 950 and 1100 °C depending on X. Total weight loss after preparation was <1.2%. The samples were characterized by metallographic examination, powder x-ray diffraction (XRD), and wavelength dispersive electron-probe microanalysis (EPMA). It was found that the samples with $X \leqslant 0.3$ contained small amounts of impurity phases $(Pt_{1-X}Pd_X)_5Al_3$ and $Ce(Pt_{1-X}Pd_X)_4Al$ [17], but the Pd composition x determined by EPMA for the main phase did not deviate from the nominal value X within the resolution. The sample with $X = 0.4$ was, however, found to be composed of four phases: $Ce(Pt_{0.66}Pd_{0.33})_6Al_3$ as the main phase and secondary phases of $Ce(Pt_{0.47}Pd_{0.49})_5Al_2$, $Ce(Pt_{0.61}Pd_{0.31})_4Al$, and $Pt_2Pd_3Al_3$. The composition of the main phase indicates the solubility limit as $x = 0.33$ in $Ce(Pt_{1-x}Pd_x)_6Al_3$. Thus, physical properties have been measured for samples with $X \leqslant 0.3$ in which the Pd composition is described as x hereafter. Lattice parameters of the $NdPt_6Al_3$-type structure were calculated by least-square refinements of the XRD patterns. The analysis of the XRD pattern indicated no preferential substitution of Pd atoms for the different Pt sites in the Ce_2Pt_3 layer and the Pt_9Al_6 block.

The measurements of $\rho(T)$, $\chi(T)$, magnetization $M(B)$, and $C(T)$ were performed by the methods as described below. A four-terminal alternating current (AC) method was used for $\rho(T)$ measurements from 0.04 to 3 K with an adiabatic demagnetization refrigerator mF-ADR50 and from 3 to 300 K with a Gifford-McMahon-type refrigerator. We used a Quantum Design SQUID magnetometer (MPMS) for the measurements of $\chi(T)$ and $M(B)$ from 1.8 to 300 K. In a lower temperature range from 0.3 to 2 K, $M(T)$ was measured by a home-built capacitively detected Faraday magnetometer in a ^{3}He cryostat [18]. The AC magnetic susceptibility $\chi_{AC}(T)$ was measured under an AC magnetic field of 300 μT

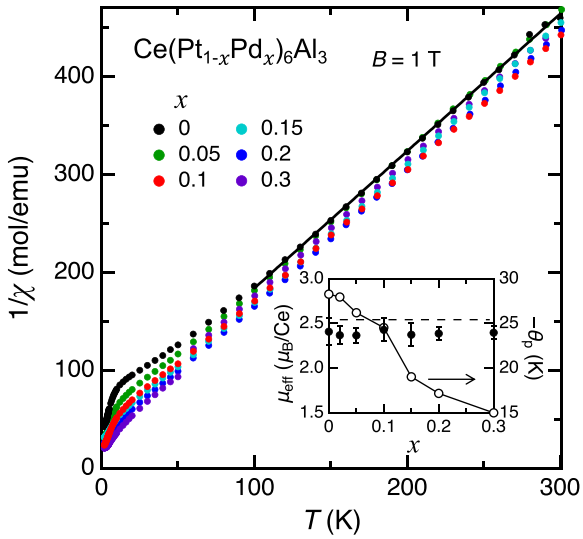

FIG. 2. Temperature dependence of the inverse of magnetic susceptibility of $Ce(Pt_{1-x}Pd_x)_6Al_3$ in a field of 1 T. The solid line is an example of the fit with the modified Curie-Weiss form $\chi = C/(T-\theta_p) + \chi_0$ to the data for $x = 0$ at temperatures >100 K. The inset shows the effective magnetic moment $\mu_{\rm eff}$ and paramagnetic Curie temperature θ_p as a function of the Pd concentration x. The horizontal broken line represents the value $\mu_{\rm eff} = 2.54\,\mu_B$ expected for a free Ce^{3+} ion.

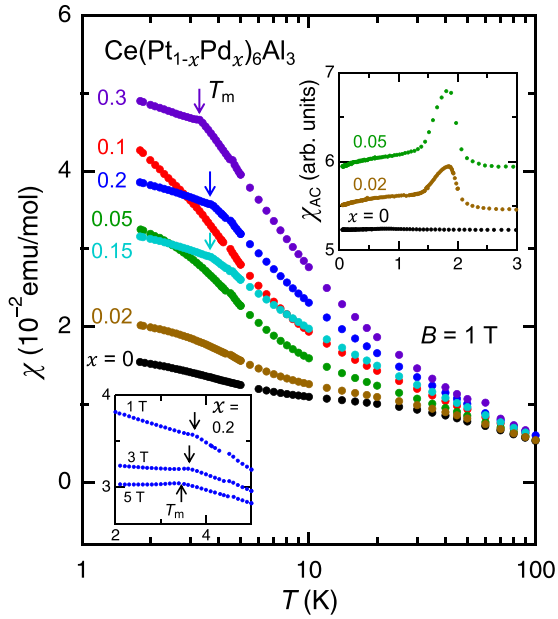

FIG. 3. Temperature dependence of the magnetic susceptibility χ of $Ce(Pt_{1-x}Pd_x)_6Al_3$ in a field of 1 T. Arrows indicate the bends in $\chi(T)$ at T_m. The lower inset shows the decrease in T_m for $x = 0.2$ with increasing the applied magnetic field to 5 T. The upper inset shows the temperature dependence of alternating current (AC) magnetic susceptibility $\chi_{\rm AC}(T)$ for $x = 0$, 0.02, and 0.05 in an AC field of 300 μT at a frequency of 4000 Hz. The data are shifted vertically for clarity.

at two frequencies of 4000 and 10 000 Hz in a Quantum Design Dynacool ^{3}He-^{4}He dilution refrigerator at University of Johannesburg. The measurement of $C(T)$ from 0.4 to 20 K was performed by the relaxation method in a Quantum Design Physical Property Measurement System (PPMS).

III. RESULTS AND DISCUSSION

As the Pd concentration x in $Ce(Pt_{1-x}Pd_x)_6Al_3$ increases from 0 to 0.3, the trigonal a parameter increases by 0.24%, while the c parameter decreases by 0.33%, as shown in Fig. 1(b). These changes in a and c result in a linear decrease in the ratio c/a by 0.57%, while keeping the unit cell volume almost constant within 0.2%, as shown in Fig. 1(c). The unchanged volume with x leads to little change in the valence state of the Ce ions, as shown next.

The inverse of χ vs T is plotted in Fig. 2, where the solid line at $T > 100$ K is the fit to the data for $x = 0$ with the modified Curie-Weiss form $\chi(T) = C/(T-\theta_p) + \chi_0$, where C is the Curie constant, θ_p is the paramagnetic Curie temperature, and χ_0 represents the temperature-independent contribution. For all samples, we assumed a constant value of $\chi_0 = -2.5 \times 10^{-4}$ emu/mol, which is the magnetic susceptibility of the nonmagnetic reference compound YPt_6Al_3 [14]. The inset of Fig. 2 shows the x dependence of $\mu_{\rm eff}$ and $-\theta_p$. In the whole range of x, the value of $\mu_{\rm eff}$ stays at 2.4 μ_B/Ce, which is close to 2.54 μ_B/Ce expected for a free Ce^{3+} ion. Therefore, no significant deviation from the trivalent state is induced by the Pd substitution. On the other hand, $-\theta_p$ gradually decreases from 28 K for $x = 0$ to 15 K for $x = 0.3$. If the frustration effect is neglected, then the decrease in $-\theta_p$ can be interpreted as the reduction of the Kondo temperature T_K [19]. Even under a constant unit cell volume, T_K may decrease if the $4f$ orbital shrinks with the isovalent substitution of Pd for Pt, as suggested for $Ce_3Bi_4(Pt_{1-x}Pd_x)_3$ [20]. As will be shown later, the reduction of T_K with increasing x is supported by the analysis of the magnetic entropy.

At low temperatures, $\chi(T)$ strongly depends on x, as shown in Fig. 3. For $0 \leqslant x \leqslant 0.1$, the $\chi(T)$ data measured in $B = 1$ T continue to increase with decreasing temperature to 1.8 K. We plot the data of $\chi_{\rm AC}(T)$ measured at a frequency of 4000 Hz for $x = 0$, 0.02, and 0.05 in the upper inset of Fig. 3. Upon cooling to 0.06 K, $\chi_{\rm AC}(T)$ for $x = 0$ shows no significant anomaly. For $x = 0.02$, $\chi_{\rm AC}(T)$ exhibits a clear peak at 1.85 K, a temperature which does not change for $x = 0.05$, but the height of the peak doubles. Note that the temperature at the peak did not shift when the frequency was increased to 10 000 Hz. This fact disagrees with a shift of peak temperature expected for a spin-glass transition [21]. We will discuss the peak in $\chi_{\rm AC}(T)$ in comparison with anomalies found in the resistivity and specific heat. When x is increased to 0.15, $\chi(T)$ sharply bends at 3.7 K, indicating a transition to a long-range magnetically ordered state. If we take the temperature at the bend as T_m, the value of T_m is unchanged as x is increased from 0.15 to 0.2, but T_m is decreased to 3.3 K for $x = 0.3$. As shown in the lower inset, T_m for $x = 0.2$ is suppressed by the applied magnetic field, a dependence which is a characteristic of an AFM order. It is noteworthy that, in strongly frustrated AFM compounds such as a quasikagome system CePdAl and a Shastry-Sutherland system Yb_2Pt_2Pb, $\chi(T)$ exhibits a broad maximum at $T \sim 1.5\,T_m$ due to the development of a short-range order above the long-range AFM transition

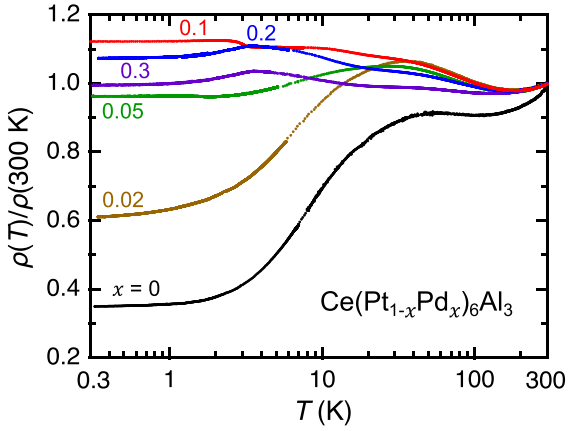

FIG. 4. Temperature dependence of electrical resistivity $\rho(T)$ normalized to the value at 300 K for $Ce(Pt_{1-x}Pd_x)_6Al_3$.

temperature [22,23]. The absence of such a maximum in $\chi(T)$ above T_m in $Ce(Pt_{1-x}Pd_x)_6Al_3$ suggests that the intersite magnetic correlation above T_m is weak compared with CePdAl and Yb_2Pt_2Pb.

Figure 4 shows the temperature dependence of electrical resistivity normalized to the value at 300 K, $\rho(T)/\rho(300\,\mathrm{K})$, for $Ce(Pt_{1-x}Pd_x)_6Al_3$. The values of $\rho(300\,\mathrm{K})$ are in the range between 130 and 150 $\mu\Omega$cm. For $x = 0$, $\rho(T)$ has a broad shoulder at ~ 60 K followed by a steep decrease, a behavior which displays the development of coherence in the Kondo lattice as observed for a single-crystalline sample [14]. For $x = 0.02$, $\rho(T)$ retains coherent behavior without showing an anomaly at 1.85 K, where $\chi_{AC}(T)$ exhibits a peak. However, the coherent behavior is lost for $x = 0.05$, as manifested by the increase in the value $\rho(0.3\,\mathrm{K})/\rho(300\,\mathrm{K})$ to 0.96. This incoherent Kondo scattering can be attributed to the local disorder in the hybridization of the Ce $4f$ state with Pt $5d$ and Pd $4d$ states. For $x = 0.1$, $\rho(T)$ continues to increase on cooling until it jumps at 3.2 K, which is better seen in Fig. 5(b). The jump hints at opening of a partial gap of the Fermi surface due to a long-range magnetic order. We will discuss this subject by combining with the specific heat data. With increasing x to 0.2, a cusp instead of a jump appears in $\rho(T)$. For $x = 0.2$ and 0.3, the $-\log T$ dependence of $\rho(T)$ in the range of 5–15 K is attributed to the incoherent Kondo scattering of conduction electrons from the doublet CEF ground state of the Ce $4f$ electron.

The data of magnetic specific heat C_m divided by T are compared with those of $\rho(T)$ in Fig. 5. For the calculation of C_m, the lattice contribution to the specific heat was subtracted by using the data for YPt_6Al_3 [14]. With decreasing $T < 2$ K, C_m/T for $x = 0$ gradually increases and passes through a maximum of 0.5 $\mathrm{J/K^2mol}$ at 0.55 K, as similarly observed for a single crystal [14]. The C_m/T curve for $x = 0.02$ continues to increase on cooling, while that for 0.05 jumps at ~ 1.8 K. This temperature agrees with those of anomalies in $\chi_{AC}(T)$ and $\rho(T)$: a peak in $\chi_{AC}(T)$ at 1.85 K in the inset of Fig. 3 and a jump in $\rho(T)$ at 1.8 K in the inset of Fig. 5(b). If we take the temperature at the jump in $\rho(T)$ as the magnetic transition temperature, T_m of 3.2 K for $x = 0.1$ is in agreement with the midpoint of the jump in C_m/T. With increasing x to 0.2 and to

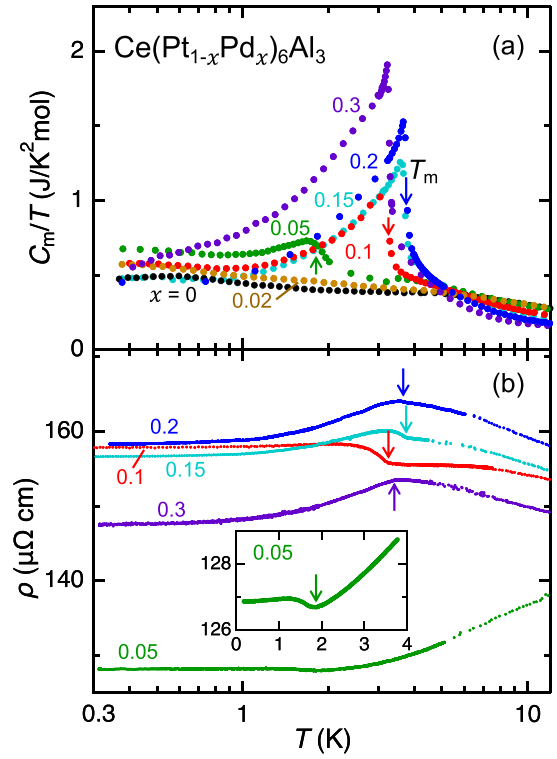

FIG. 5. (a) Magnetic part of specific heat C_m divided by temperature T and (b) electrical resistivity $\rho(T)$ for $Ce(Pt_{1-x}Pd_x)_6Al_3$ as a function of temperature. Arrows indicate the midpoint of jump in C_m/T and the anomaly in $\rho(T)$, revealing magnetic transitions at T_m. The inset shows the $\rho(T)$ data for $x = 0.05$ on an expanded scale.

0.3, the height of the jump in C_m/T further increases. The tail in C_m/T to temperatures up to twice of T_m can be attributed to short-range order at $T > T_m$. We determined the dependence of T_m on the magnetic field B from the measurements of temperature-dependent ρ and C in several constant magnetic

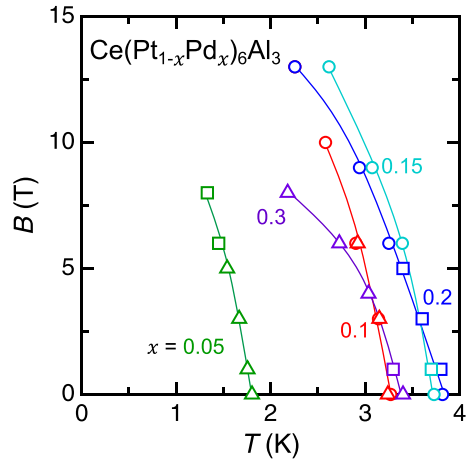

FIG. 6. Magnetic field vs temperature phase diagram for $Ce(Pt_{1-x}Pd_x)_6Al_3$ constructed from anomalies in magnetic susceptibility (open squares), specific heat (open circles), and electrical resistivity (open triangles).

fields up to 13 T. As shown in Fig. 6, T_m is gradually reduced with increasing B, as expected for an AFM transition.

Let us discuss the change in the shape of $\rho(T)$ at T_m as a function of x in relation to the magnetic order. As x is increased to 0.05, a jump in $\rho(T)$ appears, and the Kondo coherence is concurrently lost. This coincidence suggests that the magnetic order is induced by the atomic disorder in the Ce-Pt honeycomb Kondo lattice. Interestingly, the magnetic order induced by atomic disorder is opposite to the theoretical prediction on the insulating honeycomb lattice in which disorder in the NN and NNN interactions destabilizes a long-range AFM order and induces a random-singlet state [24]. The opposite behavior may arise from the Kondo effect in the present system. Note that $\rho(T)$ jumps at T_m in the dilute range $0.05 \leqslant x \leqslant 0.15$, whereas $\rho(T)$ exhibits a cusplike anomaly at T_m in the higher range $0.2 \leqslant x \leqslant 0.3$. There are two models to explain the jump in $\rho(T)$ caused by the magnetic transition. One is the SDW transition for itinerant electron systems [25]. An example is $Ce(Ru_{0.95}Rh_{0.05})_2Si_2$, in which the $4f$ electrons are involved to form the Fermi surface, as manifested in the large γ value of 0.5 J/K^2mol for the T-linear specific heat coefficient [26]. The other is the formation of a superzone gap along a certain direction of the Fermi surface depending on the wave vector of the AFM structure of localized moments [27]. An example is $CePd_5Al_2$, in which the $4f$ electrons are well localized, as manifested in the small γ value of 0.018 J/K^2 mol [28,29]. The large γ value of 0.6–0.7 J/K^2 mol for $0.05 \leqslant x \leqslant 0.15$ indirectly supports the SDW transition. The change from a jump to a cusp in $\rho(T)$ at T_m occurs between $x = 0.15$ and 0.2. With increasing x to 0.3, the cusp remains in $\rho(T)$ at $T_m = 3.2$ K. In Fig. 6, we notice that the $T_m(B)$ curve for $x = 0.3$ bends more markedly than that for $x = 0.10$ despite having almost equal value of $T_m(B = 0)$. Furthermore, as will be shown later, the magnetic entropy S_m at 5 K increases with x and reaches $0.8R\ln 2$ for $x = 0.3$, where R is the gas constant. This value of S_m means the almost full recovery of the degeneracy of the doublet ground state of localized $4f$ electron. These observations suggest a transformation from the SDW state to an AFM ordered state of more localized moments. We refer tentatively to these two states as AF I and AF II, respectively. This transformation of the ordered state with increasing x needs to be confirmed by neutron scattering experiments.

The temperature dependence of S_m gives an estimation of T_K. We calculated $S_m(T)$ by integrating the curve of C_m/T vs T in Fig. 5(a) by assuming a T-independent value at $0 \leqslant T < 0.4$ K for $x \leqslant 0.2$ and T-linear dependence for $x = 0.3$. The results of $S_m(T)/R\ln 2$ are shown in Fig. 7, and the values at 5 K are plotted in the inset. The value of $S_m(5\text{K})/R\ln 2$ increases by two times with increasing x and reaches 0.8 for $x = 0.3$, indicating large recovery of magnetic entropy of the doublet. If we neglect the effect of frustration, then T_K can be estimated by using a relation for a Kondo impurity with $\frac{1}{2}$ spin, $S(T_K) = 0.65\ln 2$ [30]. The estimated T_K decreases gradually from 10 to 3 K with the increase in x from 0 to 0.3, as shown in Fig. 8(c).

On the other hand, the frustration parameter $f = -\theta_p/T_m$ can be used as the measure of frustration [1], although θ_p and T_m are affected by the Kondo effect in the present system. As is shown in Fig. 8(d), the increase in x from 0.05 to 0.2 results

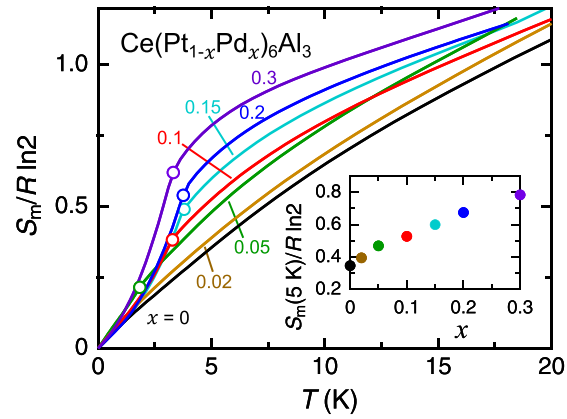

FIG. 7. Magnetic entropy S_m normalized by $R\ln 2$ for $Ce(Pt_{1-x}Pd_x)_6Al_3$ as a function of temperature. The open circles represent the values of $S_m(T)/R\ln 2$ at $T = T_m$. The inset shows the values of $S_m/R\ln 2$ at 5 K as a function of the Pd concentration x.

in the decrease in the parameter f to $\frac{1}{3}$ of the initial value, indicating the strong suppression of magnetic frustration. We conjecture that magnetic frustration of the Ce honeycomb lattice is suppressed by the atomic disorder in the Ce_2Pt_3 plane. The disorder in the Pt_9Al_6 block may have much weaker effect on the frustration because of the weak magnetic coupling between the honeycomb layers. This conjecture is based on a large difference in the spin-orbit coupling in the Pt $5d$ and Pd $4d$ states, which mediate the RKKY interaction between the Kondo screened $4f$ moments. In a quasikagome Kondo lattice YbAgGe, similar release of magnetic frustration by partial substitution of isovalent element was reported for $YbAg_{1-x}Au_xGe$ ($0 \leqslant x \leqslant 0.11$) [31]. With substituting the heavier element of Au for the lighter element of Ag, the enhancement of T_N by two times is accompanied with the decrease in the parameter f. On the contrary, T_K estimated from the magnetic entropy was found to increase with x. The opposite change in T_K and f with x for $YbAg_{1-x}Au_xGe$ is distinct from the concurrent suppression in both T_K and f observed for $Ce(Pt_{1-x}Pd_x)_6Al_3$. It is necessary to study whether the distinct behavior is due to the difference between Ce and Yb systems or due to the opposite change in the spin-orbit coupling.

Finally, we discuss the x dependences of T_m and C/T at 0.4 K, which are presented in Figs. 8(a) and 8(b), respectively. At a small level of $x = 0.02$ in $Ce(Pt_{1-x}Pd_x)_6Al_3$, only $\chi_{AC}(T)$ revealed the clear anomaly at 1.85 K, which is plotted by an open circle in Fig. 8(a). The absence of an obvious anomaly in C/T and $\rho(T)$ is a characteristic of a short-range (SR) magnetic order, and therefore, this region is denoted as SR phase. At $x = 0.05$, a long-range magnetic order sets in, as manifested by the jump in C/T and $\rho(T)$. The magnitude of C/T at 0.4 K weakly increases with x, as shown in Fig. 8(b). This weak increase is in contrast with the large enhancement of C/T in $Ce(Cu_{1-x}Au_x)_6$ near $x = 0.025$ where a long-range AFM order sets in [32]. Upon exceeding the critical concentration of Au, the $4f$ occupation number suddenly increases and leads to the breakdown of Kondo screening [33]. Note that the arrangement of Ce atoms in the monoclinic structure of $Ce(Cu_{1-x}Au_x)_6$ has no geometrical frustration. The gradual

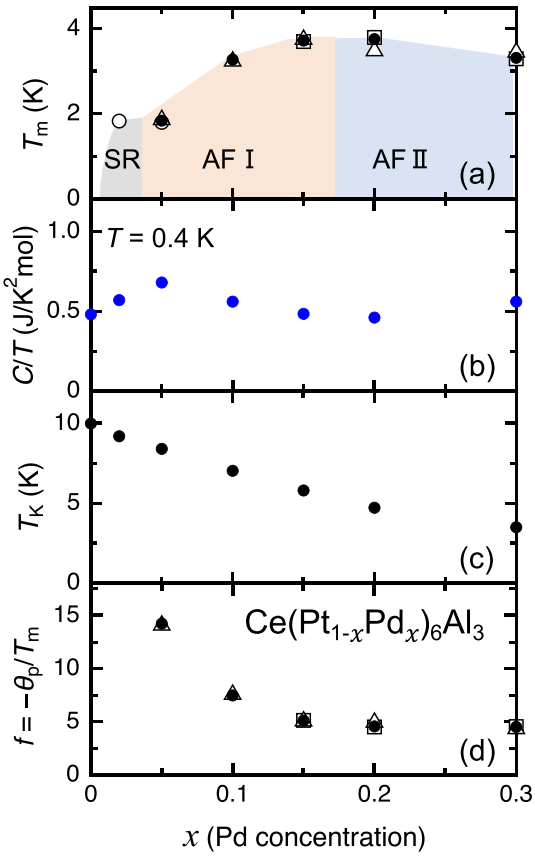

FIG. 8. Variations of physical properties of $Ce(Pt_{1-x}Pd_x)_6Al_3$ as a function of the Pd concentration x. (a) Magnetic transition temperatures T_m which are taken from anomalies in alternating current (AC) magnetic susceptibility (open circles), direct current (DC) magnetic susceptibility (open squares), specific heat (closed circles), and electrical resistivity (open triangles). SR, AF I, and AF II denote the short-range ordered state, spin-density wave (SDW) state, and antiferromagnetic (AFM) ordered state, respectively. (b) Specific heat divided by temperature C/T at 0.4 K. (c) Kondo temperature T_K estimated from the temperature-dependent magnetic entropy (see text). (d) Magnetic frustration parameter $f = -\theta_p/T_m$, where θ_p and T_m denote the paramagnetic Curie temperature and magnetic transition temperature, respectively. The marks have the same meanings as in (a).

variations of C/T and T_K with x in $Ce(Pt_{1-x}Pd_x)_6Al_3$ rule out a sudden breakdown of the Kondo screening. In the region $0.05 \leqslant x \leqslant 0.15$, T_m increases to double its value. We denote this region as AF I phase, where the jump in $\rho(T)$ at T_m is ascribed to the formation of a SDW state. With increasing x further to 0.2, the anomaly in $\rho(T)$ at T_m changes to the cusp, and $S_m(T)/R\ln 2$ at 5 K reaches 0.7. Because these features are characteristics of the AFM ordered state of rather localized $4f$ moments, we denote this region as AF II phase. The phase diagram in Fig. 8(a) is consistent with the theoretically predicted one for a frustrated Kondo lattice [9–11]. Our experimental results on $Ce(Pt_{1-x}Pd_x)_6Al_3$ corroborate the overall diagram in which a Fermi liquid state changes to an itinerant AFM ordered state and further to a local-moment AFM ordered state with the decreases in both the Kondo coupling and degree of frustration. Further experiments using single-crystalline samples are necessary to detect the partial Kondo screened state with site-dependent moment size that is predicted to occur in a frustrated Kondo system [12].

IV. CONCLUSIONS

The honeycomb Ce lattice compound $CePt_6Al_3$ is a nonmagnetic heavy-fermion system with $\gamma = 0.5\,\mathrm{J/K^2}$ mol. We have found the development of magnetic order by the substitution of isovalent Pd for Pt in $Ce(Pt_{1-x}Pd_x)_6Al_3$ ($x \leqslant 0.3$) from the transport, magnetic, and specific heat measurements. The Pd substitution does not dope charge carriers nor apply chemical pressure. In fact, in the whole range of x, the unit cell volume remains unchanged within 0.2%, and the effective magnetic moment stays at a constant value of $2.4\,\mu_B$/Ce. Nevertheless, experimental results indicate that the ground state changes from the heavy-fermion state to the SDW state and to the AFM ordered state. The ordering temperature T_m as a function of x has the maximum at 3.8 K for $x = 0.15-0.2$. We ascribe the emergence of long-range AFM order to the combination of weakening of the Kondo effect and suppression of the magnetic frustration. As for the latter mechanism, we propose that the randomness in the spin-orbit coupling in the Pt $5d$ and Pd $4d$ states modifies the periodically oscillating RKKY interaction and thus breaks the delicate balance in magnetic interactions maintaining the frustrated heavy-fermion state. To confirm this supposition, microscopic experiments by neutron scattering, muon spin relaxation, and nuclear magnetic resonance combined with band structure calculations are highly anticipated.

ACKNOWLEDGMENTS

This paper was supported by JSPS KAKENHI Grants No. JP17K05545, No. JP18H01182, and No. JP21K03473, and Iketani Science and Technology Foundation (No. 0321131-A). The SA NRF (93549) and the URC/FRC of UJ are thanked for financial assistance. The low-temperature measurements and electron-probe micro-analysis were performed at Integrated Experimental Support/Research Division, N-BARD, Hiroshima University. We acknowledge H. Kusunose and D. T. Adroja for fruitful discussions.

[1] *Frustrated Spin Systems*, 2nd ed., edited by H. Diep (World Scientific, Singapore, 2013).
[2] F. Ferrari and F. Becca, J. Phys.: Condens. Matter **32**, 274003 (2020).
[3] A. Kitaev, Ann. Phys. **321**, 2 (2006).
[4] H. Takagi, T. Takayama, G. Jackeli, G. Khaliullin, and S. E. Nagler, Nat. Rev. Phys. **1**, 264 (2019).
[5] C. Lacroix, J. Phys. Soc. Jpn. **79**, 011008 (2010).
[6] S. Hayami, H. Kusunose, and Y. Motome, Phys. Rev. B **90**, 024432 (2014).

[7] S. Hayami, H. Kusunose, and Y. Motome, J. Phys. Soc. Jpn. **84**, 064717 (2015).
[8] J. Flouquet, Prog. Low. Temp. Phys. **15**, 139 (2005).
[9] M. Vojta, Rep. Prog. Phys. **81**, 064501 (2018).
[10] P. Coleman and A. H. Nevidomskyy, J. Low Temp. Phys. **161**, 182 (2010).
[11] J. H. Pixley, R. Yu, and Q. Si, Phys. Rev. Lett. **113**, 176402 (2014).
[12] T. Sato, F. F. Assaad, and T. Grover, Phys. Rev. Lett. **120**, 107201 (2018).
[13] F. Eustermann, F. Stegemann, K. Renner, and O. Janka, Z. Anorg. Allg. Chem. **643**, 1836 (2017).
[14] R. Oishi, Y. Ohmagari, Y. Kusanose, Y. Yamane, K. Umeo, Y. Shimura, T. Onimaru, and T. Takabatake, J. Phys. Soc. Jpn. **89**, 104705 (2020).
[15] *Chemistry of the Elements*, 2nd ed., edited by N. Greenwood and A. Earnshaw (Butterworth-Heinemann, Oxford, 1997), pp. 1144–1172.
[16] S. Dzsaber, L. Prochaska, A. Sidorenko, G. Eguchi, R. Svagera, M. Waas, A. Prokofiev, Q. Si, and S. Paschen, Phys. Rev. Lett. **118**, 246601 (2017).
[17] Z. Blazona and S. M. Westwood, J. Alloys Compd. **201**, 151 (1993).
[18] T. Sakakibara, H. Mitamura, T. Tayama, and H. Amitsuka, Jpn. J. Appl. Phys. **33**, 5067 (1994).
[19] D. Gignoux and J. C. Gomez-Sal, Phys. Rev. B **30**, 3967 (1984).
[20] J. M. Tomczak, Phys. Rev. B **101**, 035116 (2020).
[21] J. A. Mydosh, *Spin Glasses: An Experimental Introduction* (Taylor & Francis, London, 1993).
[22] S. Lucas, K. Grube, C.-L. Huang, A. Sakai, W. Wunderlich, E. L. Green, J. Wosnitza, V. Fritsche, P. Gegenwart, O. Stockert, and H. v. Löhneysen, Phys. Rev. Lett. **118**, 107204 (2017).
[23] M. S. Kim, M. C. Bennett, and M. C. Aronson, Phys. Rev. B **77**, 144425 (2008).
[24] K. Uematsu and H. Kawamura, J. Phys. Soc. Jpn. **86**, 044704 (2017).
[25] E. Fawcett, Rev. Mod. Phys. **60**, 209 (1988).
[26] Y. Tabata, T. Taniguchi, M. Sato, S. Kawarazaki, and Y. Miyako, J. Phys. Soc. Jpn. **67**, 2484 (1998).
[27] A. R. Mackintosh, Phys. Rev. Lett. **9**, 90 (1962).
[28] T. Onimaru, Y. F. Inoue, K. Shigetoh, K. Umeo, H. Kubo, R. A. Ribeiro, A. Ishida, M. A. Avila, K. Ohoyama, M. Sera, and T. Takabatake, J. Phys. Soc. Jpn. **77**, 074708 (2008).
[29] T. Onimaru, Y. F. Inoue, A. Ishida, K. Umeo, Y. Oohara, T. J. Sato, D. T. Adroja, and T. Takabatake, J. Phys.: Condens. Matter **31**, 125603 (2019).
[30] H.-U. Desgranges and K. D. Schotte, Phys. Lett. A **91**, 240 (1982).
[31] K. Umeo, H. Kubo, T. Onimaru, K. Katoh, and T. Takabatake, JPS Conf. Proc. **3**, 014005 (2014).
[32] H. v. Löhneysen, M. Sieck, O. Stockert, and M. Waffenschmidt, Physica B **223-224**, 471 (1996).
[33] M. Klein, J. Kroha, H. v. Löhneysen, O. Stockert, and F. Reinert, Phys. Rev. B **79**, 075111 (2009).